Jia et al. *Zool. Res.* 2024, 45(2): 355−366
https://doi.org/10.24272/j.issn.2095-8137.2023.324

ZR | Zoological Research

Article Open Access

Androgen signaling inhibits *de novo* lipogenesis to alleviate lipid deposition in zebrafish

Jing-Yi Jia[1,2], Guang-Hui Chen[2], Ting-Ting Shu[2,3,4], Qi-Yong Lou[2], Xia Jin[2], Jiang-Yan He[2], Wu-Han Xiao[2], Gang Zhai[2,3,5,*], Zhan Yin[1,2,3,5,6,*]

[1] *College of Fisheries*, *Huazhong Agriculture University*, *Wuhan*, *Hubei* 430070, *China*
[2] *State Key Laboratory of Freshwater Ecology and Biotechnology*, *Institute of Hydrobiology*, *Chinese Academy of Sciences*, *Wuhan*, *Hubei* 430072, *China*
[3] *College of Advanced Agricultural Sciences*, *University of Chinese Academy of Sciences*, *Beijing* 100049, *China*
[4] *Hubei Key Laboratory of Three Gorges Project for Conservation of Fishes*, *Chinese Sturgeon Research Institute*, *China Three Gorges Corporation*, *Yichang*, *Hubei* 443100, *China*
[5] *Hubei Hongshan Laboratory*, *Huazhong Agriculture University*, *Wuhan*, *Hubei* 430070, *China*
[6] *Innovative Academy of Seed Design*, *Chinese Academy of Sciences*, *Beijing* 100049, *China*

ABSTRACT

Testosterone is closely associated with lipid metabolism and known to affect body fat composition and muscle mass in males. However, the mechanisms by which testosterone acts on lipid metabolism are not yet fully understood, especially in teleosts. In this study, *cyp17a1*-/- zebrafish (*Danio rerio*) exhibited excessive visceral adipose tissue (VAT), lipid content, and up-regulated expression and activity of hepatic *de novo* lipogenesis (DNL) enzymes. The assay for transposase accessible chromatin with sequencing (ATAC-seq) results demonstrated that chromatin accessibility of DNL genes was increased in *cyp17a1*-/- fish compared to *cyp17a1*+/+ male fish, including stearoyl-CoA desaturase (*scd*) and fatty acid synthase (*fasn*). Androgen response element (ARE) motifs in the androgen signaling pathway were significantly enriched in *cyp17a1*+/+ male fish but not in *cyp17a1*-/- fish. Both androgen receptor (*ar*)-/- and wild-type (WT) zebrafish administered with Ar antagonist flutamide displayed excessive visceral adipose tissue, lipid content, and up-regulated expression and activity of hepatic *de novo* lipogenesis enzymes. The Ar agonist BMS-564929 reduced the content of VAT and lipid content, and down-regulated acetyl-CoA carboxylase a (*acaca*), *fasn*, and *scd* expression. Mechanistically, the rescue effect of testosterone on *cyp17a1*-/- fish in terms of phenotypes was abolished when *ar* was additionally depleted. Collectively, these findings reveal that testosterone inhibits lipid deposition by down-regulating DNL genes via Ar in zebrafish, thus expanding our understanding of the relationship between testosterone and lipid metabolism in teleosts.

Keywords: *Cyp17a1*; Testosterone; Androgen receptor; *De novo* lipogenesis; Fatty acid synthesis

INTRODUCTION

Obesity has emerged as a worldwide epidemic, escalating the risk of cardiovascular diseases, carbohydrate and/or lipid metabolic disorders, and infertility (Broughton & Moley, 2017; Powell-Wiley et al., 2021; Rubio-Almanza et al., 2019; Safaei et al., 2021; Tonstad & Després, 2011; WHO, 2000). In mammals, lipid metabolism is closely associated with hormones, such as androgens (Kelly & Jones, 2013; Zhang et al., 2022). Notably, reduced levels of free testosterone are implicated in severe obesity through the suppression of the hypothalamic-pituitary-testicular axis, while testosterone therapy has been shown to reduce fat mass in obesity in the presence of symptomatic androgen deficiency (Aherrahrou et al., 2020; Bekaert et al., 2015; Fui et al., 2014). In men, low androgen levels are a common feature of visceral obesity and metabolic syndrome (Tchernof et al., 2018). Androgens affect various biological processes, such as adipogenesis (preadipocyte development), lipolysis, and lipid accumulation, potentially affecting body fat quantity and adipose tissue

Received: 28 November 2023; Accepted: 15 January 2024; Online: 16 January 2024
Foundation items: This work was supported by the National Key Research and Development Program, China (2022YFF1000300 to Z.Y. and 2022YFD2401800 to G.Z.), Pilot Program A Project from the Chinese Academy of Sciences (XDA24010206 to Z.Y.), Foundation of Hubei Hongshan Laboratory (2021hskf013 to G.Z. and 2021hszd021 to Z.Y.), National Natural Science Foundation of China (31972779 to G.Z.), Youth Innovation Promotion Association of CAS (2020336 to G.Z.), and State Key Laboratory of Freshwater Ecology and Biotechnology (2016FBZ05 to Z.Y.)
*Corresponding authors, E-mail: zhaigang@ihb.ac.cn; zyin@ihb.ac.cn

distribution in both sexes (Blouin et al., 2009; O'Reilly et al., 2014). Testosterone administration has been shown to significantly reduce liver fat in obese men (Hoyos et al., 2012), while dehydroepiandrosterone prevents obesity by reducing stearoyl-coenzyme a desaturase 1 (SCD1) activity in adipocytes (Karbowska & Kochan, 2013). Testosterone deficiency has also been shown to enhance diet-induced liver lipid accumulation in castrated male rats (Nikolaenko et al., 2014). Furthermore, global androgen receptor (*Ar*) knockout (*Ar*KO) mice (*Mus musculus*) or liver and hypothalamic tissue-specific *AR*KO mice, characterized by obesity with significantly elevated serum triglyceride (TG) and free fatty acid levels (Chang et al., 2013; De Gendt & Verhoeven, 2012), show elevated body fat compared to wild-type (WT) mice, alongside late onset obesity and significantly increased visceral and subcutaneous fat in males (Fan et al., 2005; Sato et al., 2003; Yanase et al., 2008). However, in comparison to mammals, the mechanisms by which testosterone acts on lipid metabolism in gene knockout fish models remains limited.

Research has indicated that exogenous androgen administration in fish influences lipid transport, lipogenesis, lipolysis, and fatty acid beta-oxidation (Divers et al., 2010; Lopes et al., 2016, 2021). Testosterone administration at certain concentrations stimulates the transcriptional expression of the key lipid regulator peroxisome proliferator-activated receptor γ (*PPARγ*) in brown trout (*Salmo trutta*) (Lopes et al., 2016), while 11-ketotestosterone (11-KT) treatment induces the transcriptional expression of hepatic lipoprotein esterase in sterlet sturgeon (*Acipenser ruthenus*) (Wang et al., 2020). Testosterone administration in Mozambique tilapia (*Oreochromis mossambicus*) has been shown to stimulate the activities of malic enzyme (ME), glucose-6-phosphate dehydrogenase (G6PDH), and isocitrate dehydrogenase (ICDH), which participate in the regulation of lipid metabolism (Sunny et al., 2002). The metabolic role of testosterone, including an increase in lipogenic capacity in the gills, and TG levels in the brain, has been reported in gilthead sea bream (*Sparus auratus*) (Sangiao-Alvarellos et al., 2006). Various studies employing genome-edited zebrafish (*Danio rerio*) to target key genes related to the steroidogenesis pathway have advanced our understanding of the relationship between androgen signaling and lipid homeostasis, establishing zebrafish as a valuable teleost model for molecular investigations of nutrient metabolism (Li et al., 2020; Sun et al., 2021; Yang et al., 2018). In zebrafish, cytochrome P450 17A1 (CYP17A1) is a critical steroidogenic enzyme essential for androgen production, while AR functions as a nuclear receptor that mediates androgen action through specific ligand binding. Based on previously generated *cyp17a1*-/- and *ar*-/- zebrafish strains, we linked androgen signaling with male-typical mating behaviors, secondary sex characters, and testicular development, and determined that increased progestin levels can restore testicular organization and spermatogenesis in fish with impaired androgen signaling (Yu et al., 2018; Zhai et al., 2017, 2018, 2022). These mutant strains provide excellent models for elucidating the molecular mechanisms by which androgen signaling influences lipid metabolism.

While chromatin immunoprecipitation sequencing (ChIP-seq) can facilitate exploration of the interactions between DNA and proteins *in vivo*, the current lack of target antibodies limits its widespread use in fish (Park, 2009). In contrast, the assay for transposase-accessible chromatin with sequencing (ATAC-seq) has been widely adopted for assessing genomic accessibility with high sensitivity (Buenrostro et al., 2013). Chromatin, serving as the gene carrier, undergoes structural remodeling with gene activation or knockout. This technique, offering a new perspective on the open regions of genomic chromatin, can help elucidate the mechanisms of transcriptional regulation across species, including fish (Beisaw et al., 2020; Luo et al., 2022). In the present study, the role of androgen signaling in lipogenesis was explored using *cyp17a1*-/- and *ar*-/- zebrafish models, as well as flutamide-treated WT male zebrafish. Based on RNA-seq and ATAC-seq analyses, results showed that androgen signaling suppressed the transcriptional expression of key enzymes involved in *de novo* lipogenesis (DNL) and alleviated lipid deposition in zebrafish.

MATERIALS AND METHODS

Animals and maintenance

The zebrafish were maintained as described previously (Westerfield, 2020). Briefly, the fish were kept in a circulated water system and maintained under standard laboratory conditions at 28.5°C with a light:dark cycle of 14:10 h. In total, 50 fish were placed in an 8 L volume tank. Fish were fed twice daily with live brine shrimp. All animal experiments were conducted in accordance with the Guiding Principles for the Care and Use of Laboratory Animals and were approved by the Institute of Hydrobiology, Chinese Academy of Sciences (Approval ID: IHB 2013724).

Knockout lines

Utilizing transcription activator-like effector nucleases (TALENs) targeting the left arm recognition sequence (5'-CTTTCAGGACCTGCAGAAGA-3') and right arm recognition sequence (5'-GTGGGAGCCCATCATGAGGG-3'), one knockout line harboring a 7 bp deletion in the first exon of *cyp17a1* was obtained. The *cyp17a1*+/- males and females were intercrossed to generate an offspring population containing *cyp17a1*+/+, *cyp17a1*+/-, and *cyp17a1*-/- genotypes (Zhai et al., 2017, 2018). The polymerase chain reaction (PCR) product containing the BglII restriction enzyme site was digested for genotyping. The putative translation products of *cyp17a1* in *cyp17a1*+/+ zebrafish contained 519 amino acids, while the knockout *cyp17a1*-/- line only retained 74 correct amino acids and exhibited premature stops after the following three incorrect amino acid residues. The *ar*+/- males and females were intercrossed to generate an offspring population containing the *ar*+/+, *ar*+/-, and *ar*-/- genotypes (Yu et al., 2018). The *cyp17a1*+/- male fish were crossed with *ar*+/- female fish to generate *cyp17a1*+/-;*ar*+/- fish, after which the *cyp17a1*+/-;*ar*+/- males and females were intercrossed to generate an offspring population containing the *cyp17a1*+/+;*ar*+/+, *cyp17a1*-/-;*ar*+/+, and *cyp17a1*-/-;*ar*-/- genotypes. To mitigate potential impacts of the ovulatory cycle on metabolic status, male zebrafish at 3 months post-fertilization (mpf) were used in the present study. The zebrafish were anesthetized using MS-222 (tricaine methane sulphonate, Sigma, USA) and sacrificed for sample collection.

Chemical reagent administration

The Ar antagonist flutamide (CAS: 13311-84-7) (Peets et al., 1974) was purchased from Selleckchem (S1908, China). Testosterone (CAS: 58-22-0) was purchased from Dr. Ehrenstorfer GmbH (C17322500, Germany). The Ar agonist

BMS-564929 (CAS: 627530-84-1) (Ostrowski et al., 2007) was purchased from MedChemExpress (HY-12111, USA). Flutamide, testosterone, and BMS-564929 were dissolved in dimethyl sulfoxide (DMSO, Sigma-Aldrich, USA) to establish stock solutions at concentrations of 724.09 mmol/L, 5 mmol/L, and 19.99 mmol/L, respectively. The stock solutions were diluted to their final concentrations at different times according to the tank system volume. The WT male zebrafish treated with flutamide (final concentration: 10 μmol/L in water) were designated as flutamide-treated WT group, while those treated with vehicle (equal volume DMSO in water) served as the control group. Treatment continued for 30 days. Male *cyp17a1*+/+;*ar*+/+, *cyp17a1*-/-;*ar*+/+, and *cyp17a1*-/-;*ar*-/- fish were administered testosterone (final concentration: 50 nmol/L) or vehicle (equal volume DMSO) for a duration of 30 days. Similarly, WT male zebrafish treated with BMS-564929 (final concentration: 200 nmol/L) were defined as the BMS-564929-treated WT group, while the control group was administered an equal volume of DMSO in water. The treatment regime lasted 30 days. Liver and whole body samples were collected for transcriptional expression analysis of genes and lipid content measurement. All fish used in chemical reagent administration were randomly selected, with six fish per group. Treatment of WT male fish with flutamide or BMS-564929 was conducted in quadruplicate and triplicate, respectively, with measurements taken from fish in these groups. Treatments of *cyp17a1*+/+;*ar*+/+, *cyp17a1*-/-;*ar*+/+, and *cyp17a1*-/-;*ar*-/- fish with testosterone were performed in duplicate, with measurements taken from fish in these groups. Fish were fed twice daily with live brine shrimp and all samples were obtained 2 h after feeding.

TG measurement, Nile Red staining, and lipid content quantification

Visceral mass and muscle TG were measured using a Triglyceride Assay Kit (A110-1-1, Nanjing Jiancheng Bioengineering Institute Co., Ltd., China) following the manufacturer's instructions. Neutral lipid staining was performed using Nile Red dye (N3013, Sigma, USA) at a working concentration of 0.1 μg/mL for 12 h in the dark, followed by acquisition of fluorescent images using an Olympus SZX16FL stereomicroscope (Olympus, Japan) at an excitation wavelength of 488 nm (Xi et al., 2023; Yang et al., 2018). Total lipid content (percent dry weight) was measured using the Folch method (Folch et al., 1957). Briefly, individual vacuum freeze-dried zebrafish were cut up in 5 mL of chloroform (Sinopharm Chemical Reagent Co., Ltd., China):methanol (Sinopharm Chemical Reagent Co., Ltd., China) (2:1, vol/vol), extracted for 2 h, and centrifuged at 750 ×*g* for 5 min at room temperature. The upper phase was then vortexed with 0.4% calcium chloride (Sinopharm Chemical Reagent Co., Ltd., China), with the upper water phase discarded and the lower organic phase dried and weighed to measure total lipid mass per fish.

Enzyme activity measurements

Lipogenic enzyme assays were conducted according to previous study (Chen et al., 2013). Briefly, liver samples were homogenized in 20-fold volumes of ice-cold lysis buffer, and centrifuged at 13 000 ×*g* for 15 min at 4°C. The supernatant was collected separately and immediately used for enzymatic analysis using a spectrophotometer (Molecular Devices, USA). Changes in absorbance at 340 nm were monitored at intervals of 15 s for 15 min. The lipogenic enzyme activities of 6-phosphogluconate dehydrogenase (6PGD, EC:1.1.1.44), glucose-6-phosphate dehydrogenase (G6PD, EC:1.1.1.49), isocitrate dehydrogenase (ICDH, EC:1.1.1.42), and fatty acid synthase (FAS, EC:2.3.1.85) were measured. One unit of enzyme activity (IU), defined as the amount of enzyme converting 1 μmol of substrate into product per min at 28°C, was expressed as units per milligram (mg) of soluble protein.

Free fatty acid composition analysis

Muscle and liver samples were harvested from *cyp17a1*-/- and *cyp17a1*+/+ fish for free fatty acid composition analysis, as described in previous research (Tan et al., 2020; Ubhayasekera et al., 2013). The samples (50 mg) were mixed with 150 μL of methanol (Darmstadt, Germany), 200 μL of methyl tert-butyl ether (Darmstadt, Germany), and 50 μL of 36% phosphoric acid (Sigma-Aldrich, USA)/water (Millipore, USA), then vortexed for 3 min at 580 ×*g*, followed by centrifugation at 13 500 ×*g* for 5 min at 4°C. The collected supernatant (200 μL) was transferred to a new centrifuge tube, evaporated to dryness, reconstituted with 300 μL of a 15% boron trifluoride (RHAWN, China) methanol solution, vortexed for 3 min at 580 ×*g*, and incubated in an oven at 60°C for 30 min. After cooling to room temperature, 500 μL of n-hexane (Darmstadt, Germany) and 200 μL of saturated sodium chloride (Sigma-Aldrich, USA) solution were added, after which the solution was vortexed for 3 min and centrifuged at 13 500 ×*g* for 5 min at 4°C, with 100 μL of n-hexane layer solution then taken for subsequent GC-MS analysis using the Agilent 7890B-7000D GC-MS/MS platform (Agilent, USA). Fatty acids were identified by retention times of standard mixtures (Personal Bio, China). Details on GC-EI-MS/MS procedures and assays are provided in the Supplementary Materials.

RNA extraction and quantitative real-time polymerase chain reaction (qPCR)

Total RNA was extracted from the liver of zebrafish using TRIzol reagent (Invitrogen, USA). Total RNA (1 μg) was reverse transcribed into cDNA using an EasyScript One-Step gDNA Removal and cDNA Synthesis Super Mix Kit (Beijing TransGen Biotech, China). The qPCR was performed using the CFX Connect Real-Time System (Bio-Rad Systems, USA). *β-actin* was used as the housekeeping gene for normalization of gene expression levels and data were analyzed as described previously (Livak & Schmittgen, 2001). Details on primer sequences of ATP-citrate lyase a (*aclya*), acetyl-CoA carboxylase a (*acaca*), fatty acid synthase (*fasn*), stearoyl-CoA desaturase (*scd*), *β-actin* used in the present study were provided in Table 1.

RNA-seq and analysis

RNA-seq reads were generated using the Illumina HiSeq™ 3000 system (Illumina, USA). High-quality mRNA reads were mapped to the *Danio rerio* genome (GRCz11) using HISAT2 (v.2.2.0) (Kim et al., 2019). Gene expression was measured based on fragments per kilobase of exons per million mapped reads (FPKM). Differentially expressed genes (DEGs) were determined by DESeq2 (v.1.20.0) (Love et al., 2014). Kyoto Encyclopedia of Genes and Genomes (KEGG) pathway enrichment analysis and Gene Set Enrichment Analysis (GSEA) were performed using the clusterProfiler package (v.3.18.1) (Yu et al., 2012). Differential expression patterns of genes were further validated by qPCR analysis (Table 1; Supplementary Materials).

Table 1 Primers used for qPCR in this study

Gene	Accession No.	Primers (5'-3')	Product size (bp)
aclya	BC076484.1	F: AGACCTGATCTCCAGCCTCACATC R: ATGCCACTGTCGAATGCCTTACTG	108
acaca	NM_001271308	F: GGACGGACCCTTGCACAATA R: CCTCTGCAGGTCGATACGTC	91
fasn	XM_009306806	F: GAGAAAGCTTGCCAAACAGG R: GAGGGTCTTGCAGGAGACAG	203
scd	NM_198815	F: TTCTGGCCATCGGAAACTCC R: TCTCTCGATGACTTCCGGGT	179
β-actin	AY222742	F: GTCATCACCATTGGCAAT R: CGTGGATACCGCAAGATT	88

aclya, ATP-citrate lyase a; *acaca*, acetyl-CoA carboxylase alpha; *fasn*, fatty acid synthase; *scd*, stearoyl-CoA desaturase; *β-actin*, *acta1b*: actin alpha 1, skeletal muscle b.

ATAC-seq and analysis

The ATAC-seq libraries were prepared as described previously (Buenrostro et al., 2015). Firstly, liver nucleic suspensions were incubated in a transposition (Tn5) mix that included a transposase, followed by DNA purification and fragment sorting. Finally, the primary libraries were obtained by amplifying the captured DNA using adapter primers and sequenced using the Illumina HiSeq^{TM} 4000 system (Illumina, USA; Supplementary Materials). The quality of the raw data was determined using FastQC (v.0.11.5), with Trim Galore (v.0.6.7) used to obtain high-quality clean reads. Bowtie2 (v.2.3.5.1) was then used to map the clean reads to the *Danio rerio* reference genome (GRCz11) with the parameter " –X 2000". Peak calling was performed using MACS3 software (v.3.0.0a7). Differential peaks (DPs) were analyzed by edgeR (v.3.32.11) with cutoff criteria of $|\log_2 FC| \geq 2$ and false discovery rate (FDR)<0.05. Visualization of peaks was performed using integrative genomics viewer (IGV) tools. Genes corresponding to the DPs of each sample were identified and annotated with the ChIPseeker package (v.1.28.3) (Yu et al., 2015). The motifs in DPs of each sample were examined using the findMotifsGenome.pl tool in HOMER (v.4.11) (Supplementary Materials).

Integrative analysis of ATAC-seq and RNA-seq

Transcription factor (TF) binding sites were identified using ATAC-seq data. To explore the gene expression levels of TFs and their regulatory roles in gene expression, the ATAC-seq and RNA-seq data were integrated. Genes associated with the open chromatin regions in *cyp17a1*-/- and *cyp17a1*+/+ fish overlapped with the up- and down-regulated genes identified with RNA-seq.

Statistical analysis

All statistical analyses were performed using R (v.4.0.2) (Team, 2021), with results expressed as mean±standard deviation (SD). GraphPad Prism v.9.0 (GraphPad Software, USA) was used to visualize the data. Two-tailed Student's *t*-test or one-way analysis of variance (ANOVA) and Turkey's test were used to assess differences between groups. For all statistical comparisons, $P<0.05$ was used to indicate a statistically significant difference, with significance set to: *: $P<0.05$; **: $P<0.01$; ***: $P<0.001$.

RESULTS

***Cyp17a1*-/- fish exhibited excessive visceral adipose tissue (VAT) and up-regulated lipogenesis-related enzyme expression and activity in the liver**

Intercrossing *cyp17a1*+/- males and females generated offspring with *cyp17a1*+/+, *cyp17a1*+/-, and *cyp17a1*-/- genotypes in a Mendelian inheritance ratio of 1:2:1 (Zhai et al., 2017, 2018). The *cyp17a1*-/- zebrafish lacking functional androgen were used to characterize lipid metabolism patterns. Compared with the male *cyp17a1*+/+ fish, the *cyp17a1*-/- fish showed increased body weight (Figure 1A). Whole-body lipid staining using Nile Red revealed more VAT accumulation in *cyp17a1*-/- males than in *cyp17a1*+/+ males (Figure 1B, C). Lipid content was significantly increased in *cyp17a1*-/- fish compared to *cyp17a1*+/+ fish (Figure 1D). Comparative analysis of lipid content was conducted in body weight-matched *cyp17a1*+/+ (0.2367±0.0081 g) and *cyp17a1*-/- (0.2365±0.0098 g) individuals, showing that lipid content was significantly higher in *cyp17a1*-/- fish than body weight-matched *cyp17a1*+/+ fish (31.19%±4.05% vs. 25.22%±4.70%, respectively) (Supplementary Table S1). Furthermore, TG content was higher in visceral mass than in muscle in the *cyp17a1*-/- fish (Figure 1E).

To determine the mechanism related to elevated lipid content in *cyp17a1*-/- male zebrafish, hepatic transcriptome analyses were performed. A total of 367 significant DEGs were identified in the *cyp17a1*-/- fish liver compared to the *cyp17a1*+/+ male fish liver, including 171 significantly up-regulated and 196 significantly down-regulated genes (Supplementary Table S2). Among these genes, lipogenesis-related genes were significantly up-regulated in the *cyp17a1*-/- fish liver, including *aclya*, *acaca*, *fasn*, *scd*, *elovl6*, and *acsbg2* (Figure 1F). In addition, the transcriptional expression of key enzymes involved in DNL was significantly up-regulated in *cyp17a1*-/- fish liver, including *aclya*, *acaca*, *fasn*, and *scd*, as verified by qPCR (Figure 1G). GSEA also indicated that lipid synthesis of the fatty acid metabolic pathway was significantly activated in the liver of *cyp17a1*-/- fish (Figure 1H). Activities of the 6PGD, G6PD, ICDH, and FAS metabolic enzymes, which regulate NADPH production and are essential for fatty acid biosynthesis, were measured and found to be significantly increased in *cyp17a1*-/- fish compared to male *cyp17a1*+/+ fish (Figure 1I). As the rate-limiting enzyme in monounsaturated fatty acid synthesis, *scd* promotes the conversion of stearic acid (C18:0) into oleic acid (C18:1) in DNL. Notably, the stearic to oleic acid desaturation index (ratio of stearic product to oleic desaturation substrate, C18:1/C18:0) was increased in *cyp17a1*-/- fish compared to male *cyp17a1*+/+ fish (Figure 1J).

Landscapes of genomic chromatin accessibility in androgen signaling deficiency model

ATAC-seq, widely used to provide a sensitive assessment of

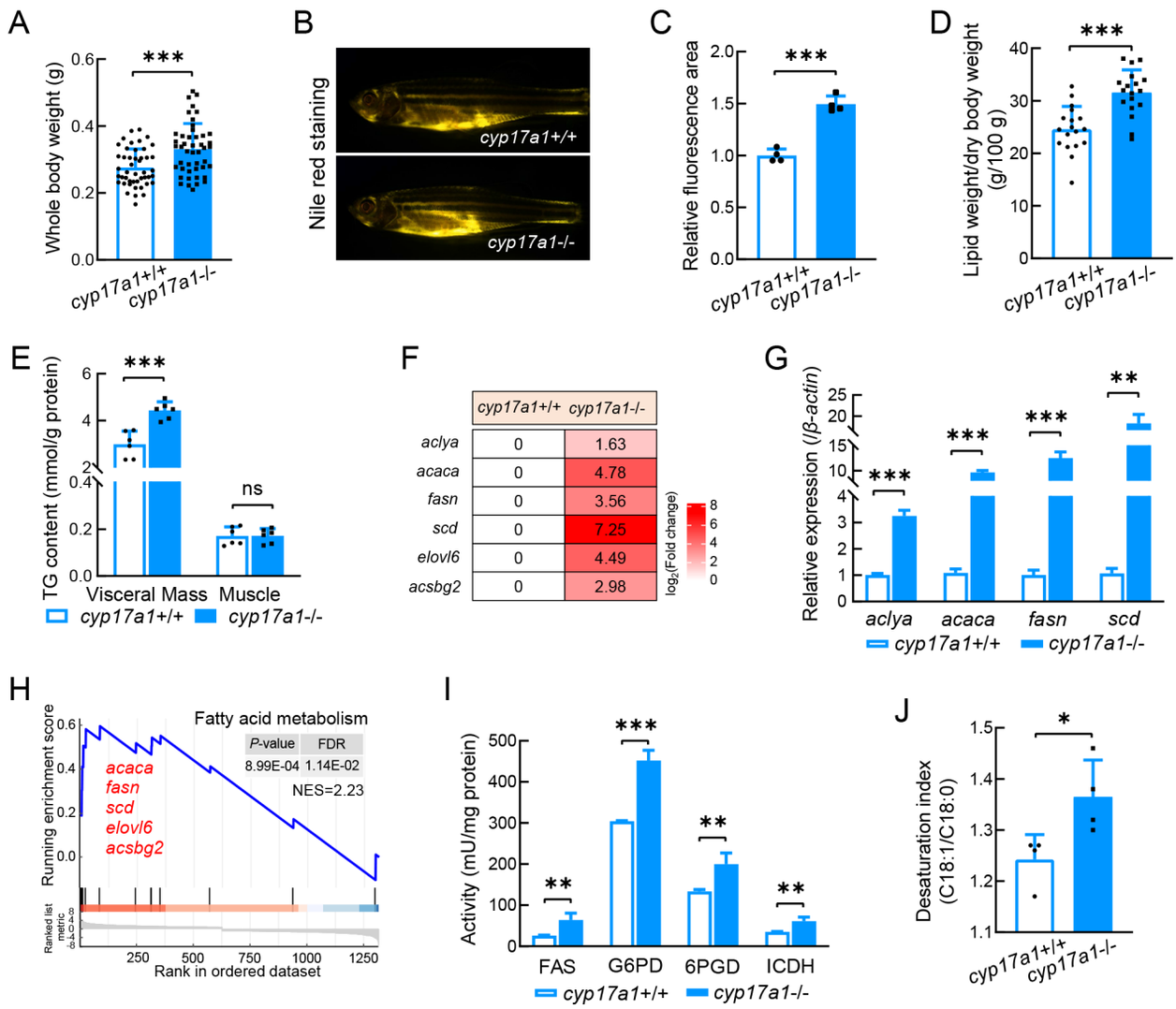

Figure 1 Characterization of lipid metabolism in *cyp17a1*-/- fish

A: Whole-body weight of male *cyp17a1*+/+ and *cyp17a1*-/- fish (*n*=46/group). B: Nile red staining of male *cyp17a1*+/+ and *cyp17a1*-/- fish. C: Quantification of fluorescence area in Nile red staining of male *cyp17a1*+/+ and *cyp17a1*-/- fish (*n*=4/group). D: Whole-body lipid content in male *cyp17a1*+/+ and *cyp17a1*-/- fish (*n*=18/group). E: Visceral mass and muscle TG content in male *cyp17a1*+/+ and *cyp17a1*-/-fish (*n*=6/group). TG, triglyceride. F: Heatmap of lipogenesis-related genes in male *cyp17a1*+/+ and *cyp17a1*-/- fish. G: qPCR of *de novo* lipogenesis (DNL)-related genes in male *cyp17a1*+/+ and *cyp17a1*-/- fish (*n*=9/group). H: KEGG pathway GSEA of liver RNA-seq data in male *cyp17a1*+/+ and *cyp17a1*-/- fish. NES: Enrichment score after normalization. I: Analysis of hepatic *de novo* lipogenic enzyme activity in male *cyp17a1*+/+ and *cyp17a1*-/- fish (*n*=5/group). J: Stearic to oleic desaturation index (C18:1/C18:0) in male *cyp17a1*+/+ and *cyp17a1*-/- fish (*n*=4/group). Data represent mean±SD. ns: Not significant; *: $P<0.05$; **: $P<0.01$; ***: $P<0.001$.

genomic accessibility (Buenrostro et al., 2013), was applied to analyze the impact of androgen signaling deficiency on chromatin openness. The distribution of ATAC-seq fragment sizes displayed the expected pattern, with a prevalence of short (<200 bp) fragments corresponding to nucleosome-free regions and progressively fewer large fragments (≥200 bp) corresponding to open chromatin spanning nucleosomes (Supplementary Figure S1A), confirming the high quality of the ATAC-seq data. The identified chromatin open regions were mostly enriched within 3 kb of the transcription start site (TSS) and centered at the TSS (Supplementary Figure S1B), indicating that TFs likely bind to these regions.

Among all ATAC-seq samples, a total of 113 349 nucleosome-free regions (peaks) were identified within the zebrafish genome. Differential peak intensity analyses identified 492 and 655 more accessible peaks in the male *cyp17a1*+/+ and *cyp17a1*-/- fish, respectively (Supplementary Table S3). Among these differential peaks, approximately 13%–15% were located 3 kb upstream of a TSS, 24%–30% were located in intergenic regions, and 57%–60% were located in introns, exons, and untranslated regions (UTRs) of gene bodies (Figure 2A, B). Chromatin openness in the promoter region of the gene was further analyzed to elucidate gene regulatory relationships and functional differences in expression regulation between genes associated with differential peaks in the promoter region were determined using KEGG pathway enrichment analysis. Results showed that the glycerophospholipid, glycerolipid, and fatty acid metabolism pathways were significantly enriched in *cyp17a1*-/- fish (Figure 2C). Notably, within the fatty acid metabolism pathway, two key DNL-related genes, *scd* and *fasn*, exhibited marked differences in chromatin accessibility profiles between the male *cyp17a1*+/+ and *cyp17a1*-/- fish, as observed by IGV analysis (Figure 2D, E).

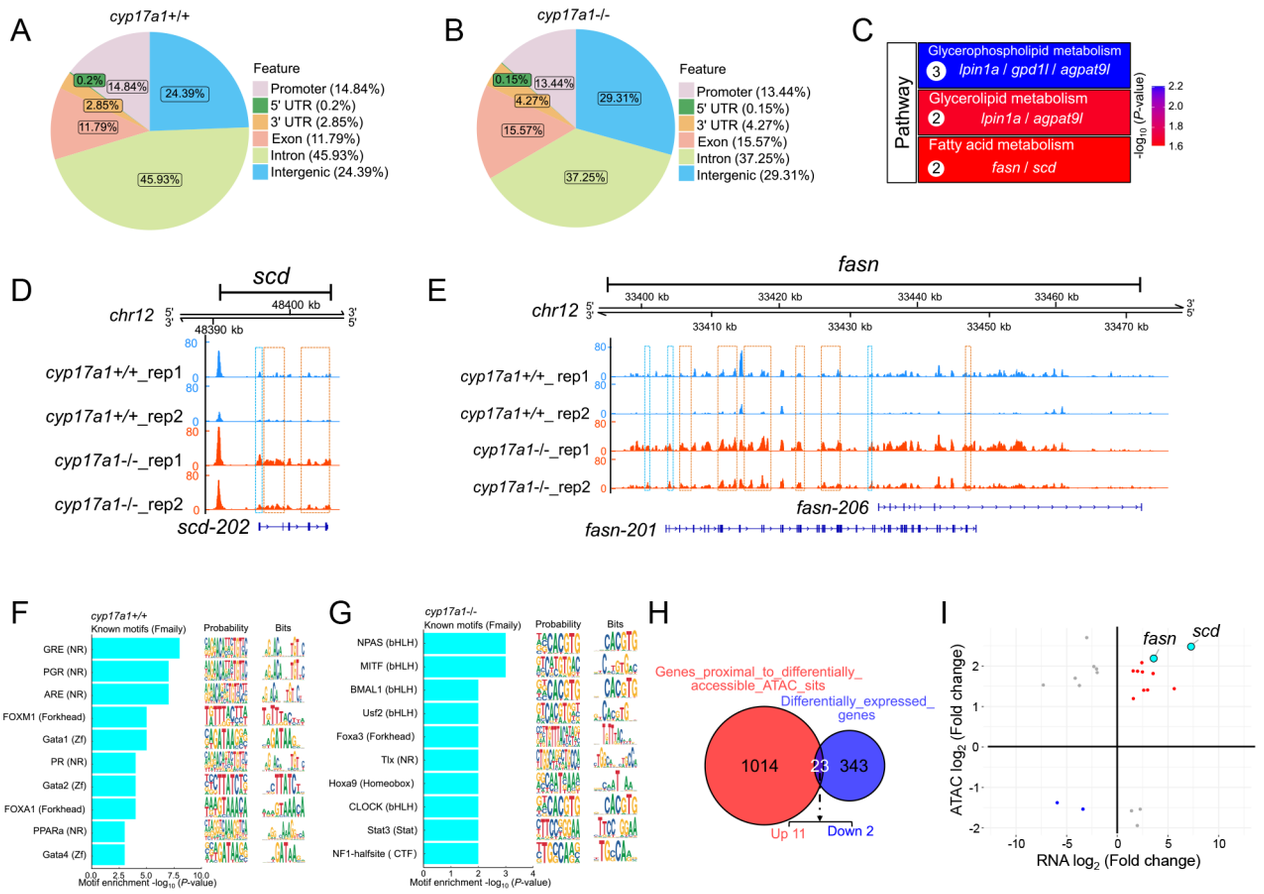

Figure 2 Differential analysis of liver-specific ATAC-seq data in *cyp17a1*-/- fish

A: Distribution of differential peaks with reduced chromatin accessibility in *cyp17a1*-/- fish genome. B: Distribution of differential peaks with enhanced chromatin accessibility in *cyp17a1*-/- fish genome. C: KEGG pathway enrichment analysis of genes related to enhanced chromatin accessibility in promoter region in liver of *cyp17a1*-/- fish. White dots represent number of differentially peak-related genes. Background colors represent significance (*p*-value). D: IGV visualization of *scd*-normalized ATAC-seq signals. E: IGV visualization of *fasn*-normalized ATAC-seq signals. Light blue dashed boxes represent differential peaks in defined genomic promoter regions. Orange dashed boxes represent differential peaks in genomic regions other than promoter regions. F: Top 10 significantly enriched motifs in *cyp17a1*+/+ fish in differential chromatin open regions. G: Top 10 significantly enriched motifs in *cyp17a1*-/- fish in differential chromatin open regions. H: Venn analysis of ATAC-seq and RNA-seq. Up: up-regulated. Down: down-regulated. I: Scatter plot of differential chromatin open regions and DEGs. Red dots: co-up-regulated. Blue dots: co-down-regulated. ATAC-seq samples include two replicates per group and three livers per replicate.

To identify potential reasons for variations in chromatin accessibility, HOMER analysis was used to detect over-represented DNA motifs indicative of putative TF binding within regions of differential accessibility in promoters. The top 10 enriched TF motifs in differentially accessible regions were identified in male *cyp17a1*+/+ and *cyp17a1*-/- fish. Notably, the NR family (GRE, PGR, ARE, PR, and PPARa), Forkhead family (FOXM1 and FOXA1), and Zf family (Gata1, Gata2, and Gata4) were the most enriched motifs in male *cyp17a1*+/+ fish (Figure 2F), whereas the bHLH family (NPAS, MITF, BMAL1, Usf2, and CLOCK), Forkhead family (Foxa3), NR family (Tlx), Homeobox family (Hoxa9), Stat family (Stat3), and CTF family (NF1-half site) were the most enriched motifs in *cyp17a1*-/- fish (Figure 2G). Interestingly, the ARE motif associated with the androgen signaling pathway was not enriched in *cyp17a1*-/- fish but was observed in male *cyp17a1*+/+ fish (Figure 2F).

Integrative analysis of lipogenesis-related chromatin openness and gene transcriptional expression in *cyp17a1*-/- fish

Integrative ATAC-seq and RNA-seq analyses were performed in *cyp17a1*-/- zebrafish to characterize the potential regulatory relationship between chromatin accessibility and differential gene expression. Venn analysis identified 23 intersecting genes, 13 of which exhibited concordance with chromatin accessibility changes (Figure 2H; Supplementary Table S4). Among these, the transcriptional levels of *fasn* and *scd*, two key genes related to DNL, were among the 11 positively correlated patterns observed between differential expression and chromatin accessibility. Both were significantly up-regulated in parallel with alterations in chromatin accessibility. This suggests that the Fasn and Scd enzymes may be key targets of the androgen signaling pathway, contributing to enhanced DNL, VAT, and lipid content in *cyp17a1*-/- zebrafish (Figure 2I).

***ar*-/- and flutamide-treated fish exhibited excessive VAT and up-regulated lipogenesis-related enzyme expression and activity in the liver**

We hypothesized that the reduction in ARE motifs in the open regions of chromatin in *cyp17a1*-/- fish may be related to dysregulated lipid metabolism mediated by insufficient Ar activation. Intercrossing of *ar*+/- males and females generated offspring with *ar*+/+, *ar*+/-, and *ar*-/- genotypes in a Mendelian

inheritance ratio of 1:2:1 (Yu et al., 2018). Lipid homeostasis was assessed in male *ar*-/- and *ar*+/+ zebrafish, revealing that *ar*-/- males exhibited increased body weights (Figure 3A), greater VAT (Figure 3B, C) and elevated body lipid content (Figure 3D) compared to *ar*+/+ males. Body weight-matched individuals were selected for further comparison, showing that lipid content was still significantly higher in *ar*-/- fish (0.2297±0.0214 g) than in *ar*+/+ fish (0.2190±0.0152 g) (25.08%±2.78% vs. 19.79%±1.00%, respectively) (Supplementary Table S5). Furthermore, TG content was found to be higher in visceral mass compared to muscle in *ar*-/- fish (Figure 3E). Therefore, the phenotype of male *ar*-/- fish was comparable to that of *cyp17a1*-/- fish when each was contrasted with their respective siblings.

RNA-seq analyses identified a total of 211 significant hepatic DEGs in male *ar*-/- fish compared to male *ar*+/+ fish, including 101 significantly up-regulated and 110 significantly down-regulated genes (Supplementary Table S6). The significantly up-regulated DEGs detected in *ar*-/- fish included several key genes involved in DNL, such as *acaca*, *fasn*, *scd*, *elovl2*, *elovl6*, and *acsbg2* (Figure 3F), with four genes further verified by qPCR (Figure 3G). GSEA indicated that lipid synthesis of the fatty acid metabolic pathway was significantly activated in *ar*-/- fish (Figure 3H), as were the activities of the several key liver lipogenic enzymes, including FAS, G6PD, 6PGD and ICDH (Figure 3I).

To further confirm the phenotypes after *ar*- depletion, male WT fish at 3 mpf were selected for administration of Ar antagonist flutamide (Peets et al., 1974). Increased VAT and whole-body lipid content were observed in the flutamide-treated WT fish (Figure 4A–C). Lipogenesis-related genes, including *aclya*, *acaca*, *fasn*, *scd*, *elovl2*, *elovl6*, *acsbg2*, and *fads2*, were also significantly up-regulated in the livers of flutamide-treated WT fish compared to WT fish based on RNA-seq and qPCR analyses (Figure 4D, E). GSEA also indicated that the hepatic DNL metabolic pathway was significantly activated in flutamide treated WT fish (Figure 4F).

RNA-seq analyses of *cyp17a1*-/- fish (compared to *cyp17a1*+/+ fish), *ar*-/- fish (compared to *ar*+/+ fish), and flutamide-treated WT fish (compared to WT fish) were subjected to Venn analysis to obtain candidate cohort regulatory gene sets after androgen signaling blockade. Results identified a total of eight overlapping genes co-regulated in the three comparison models, including significantly up-regulated genes (*acaca*, *fasn*, *scd*, *elvol6*, and *acsbg2*) related to hepatic lipogenesis (Figure 5A, B). These findings indicate that both disrupting androgen synthesis and inhibiting androgen signaling through Ar inactivation similarly promote lipid accumulation.

Testosterone treatment rescued excessive VAT, lipid content, and up-regulated *acaca*, *fasn*, and *scd* in *cyp17a1*-/- fish

The Ar agonist BMS-564929 (Ostrowski et al., 2007) was administered to WT zebrafish from 3 mpf to 4 mpf, resulting in reduced VAT and lipid content and down-regulated *acaca*, *fasn*, and *scd* expression (Figure 6A–D). Subsequently, testosterone was administered to the male *cyp17a1*+/+;*ar*+/+, *cyp17a1*-/-;*ar*+/+, and *cyp17a1*-/-;*ar*-/- zebrafish to analyze VAT content, lipid content, and DNL gene expression. Results showed that testosterone administration in *cyp17a1*+/+;*ar*+/+ fish reduced VAT and lipid content and down-regulated *acaca*, *fasn*, and *scd* expression (Figure 6E–H (White)). Furthermore, increased VAT and lipid content and up-regulated *acaca*, *fasn*, and *scd* expression were rescued in *cyp17a1*-/-;*ar*+/+fish following testosterone treatment (Figure 6E–H (Purple)); however, the rescuing effects of testosterone on VAT content, lipid content, and DNL gene expression were abolished when *ar* was additionally depleted in *cyp17a1*-/-;*ar*-/- zebrafish (Figure 6E–H (Cyan)).

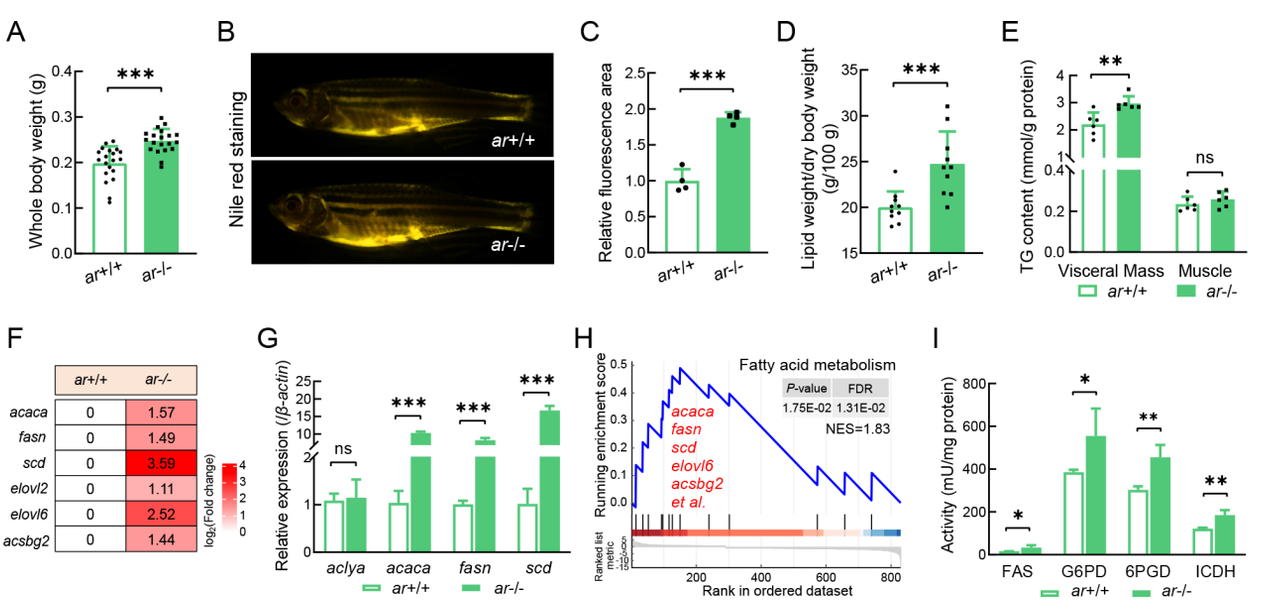

Figure 3 Characterization of lipid metabolism in *ar*-/- fish

A: Whole-body weights of male *ar*+/+ and *ar*-/- fish (*n*=20/group). B: Nile red staining of male *ar*+/+ and *ar*-/- fish. C: Quantification of fluorescence area in Nile red staining of male *ar*+/+ and *ar*-/- fish (*n*=4/group). D: Whole-body lipid content in male *ar*+/+ and *ar*-/- fish (*n*=10/group). E: Visceral mass and muscle TG content in male *ar*+/+ and *ar*-/- fish (*n*=6/group). TG, triglyceride. F: KEGG pathway GSEA of liver RNA-seq data male *ar*+/+ and *ar*-/- fish. NES: Enrichment score after normalization. G: Heatmap of lipogenesis-related genes in male *ar*+/+ fish and *ar*-/- fish. H: qPCR of hepatic DNL-related genes in male *ar*+/+ and *ar*-/- fish (*n*=9/group). I: Analysis of hepatic *de novo* lipogenic enzyme activity in male *ar*+/+ and *ar*-/- fish (*n*=5/group). Data represent mean±SD. ns: Not significant; *: $P<0.05$; **: $P<0.01$; ***: $P<0.001$.

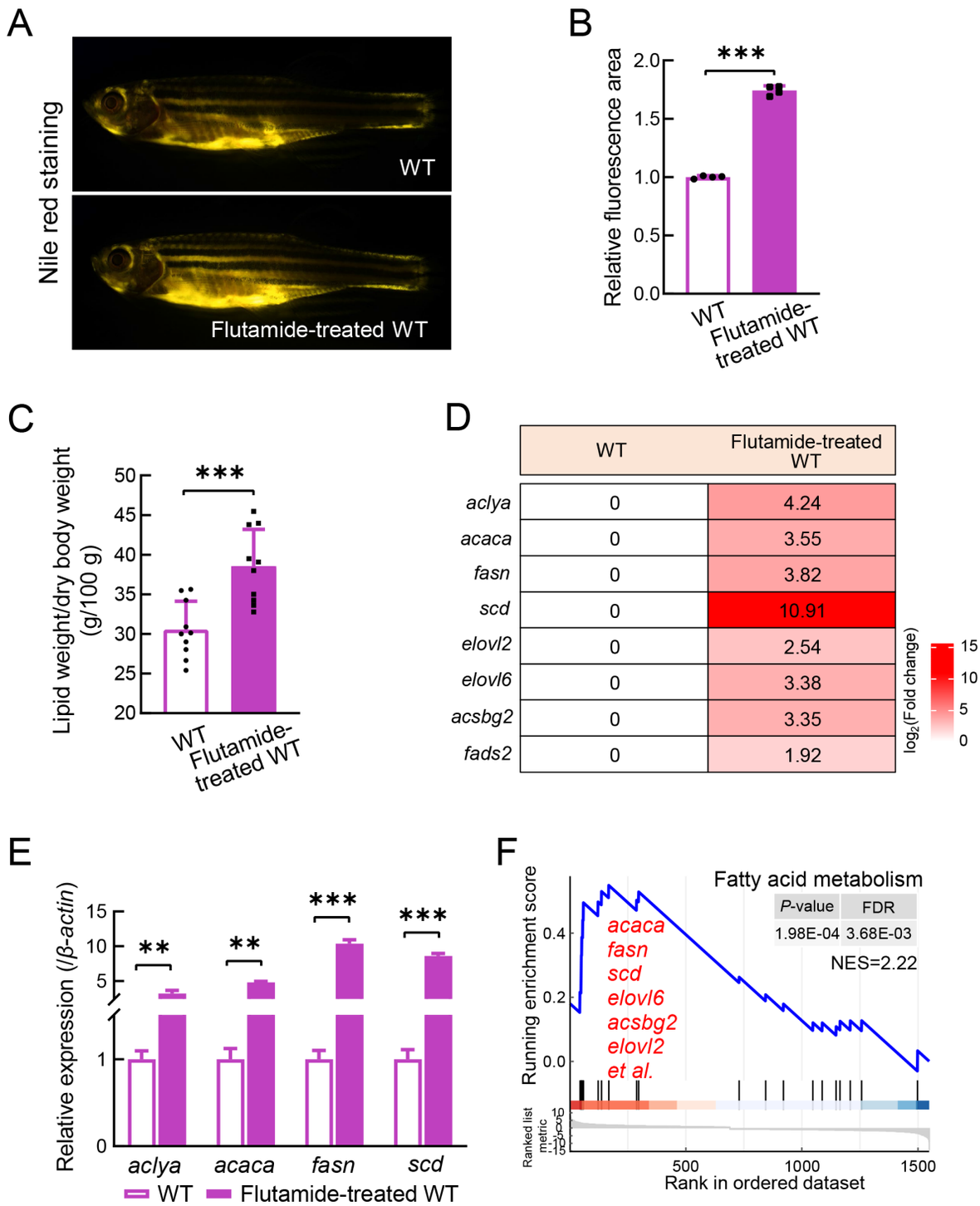

Figure 4 Characterization of lipid metabolism in flutamide-treated WT fish

A: Nile red staining of male WT and flutamide-treated WT fish. B: Quantification of fluorescence area of Nile red staining in male WT and flutamide-treated WT fish (*n*=4/group). C: Whole-body lipid content in male WT and flutamide-treated WT fish (*n*=10/group). D: Heatmap of hepatic DNL-related genes in male WT and flutamide-treated WT fish. E: qPCR of lipogenesis-related genes in male WT and flutamide-treated WT fish (*n*=4/group). F: KEGG pathway GSEA of liver RNA-seq data in male WT and flutamide-treated WT fish. NES: Enrichment score after normalization. Data represent mean±SD. **: P<0.01; ***: P<0.001.

DISCUSSION

Despite extensive research into the association between androgen signaling and lipid metabolism, the specific mechanisms in fish remain incompletely understood. In this study, we investigated the role of androgen signaling in DNL using zebrafish models of androgen signaling deficiency, including *cyp17a1*-/-, *ar*-/-, and flutamide-treated WT fish. These models demonstrated increased body weight, elevated body lipid accumulation, and up-regulated transcriptional expression and enzyme activity of DNL-related molecules.

The *cyp17a1*-/- and *ar*-/- zebrafish generated in our laboratory showed impaired male-typical secondary sex characteristics resulting from depletion of androgen signaling via distinct mechanisms (Yu et al., 2018; Zhai et al., 2018;

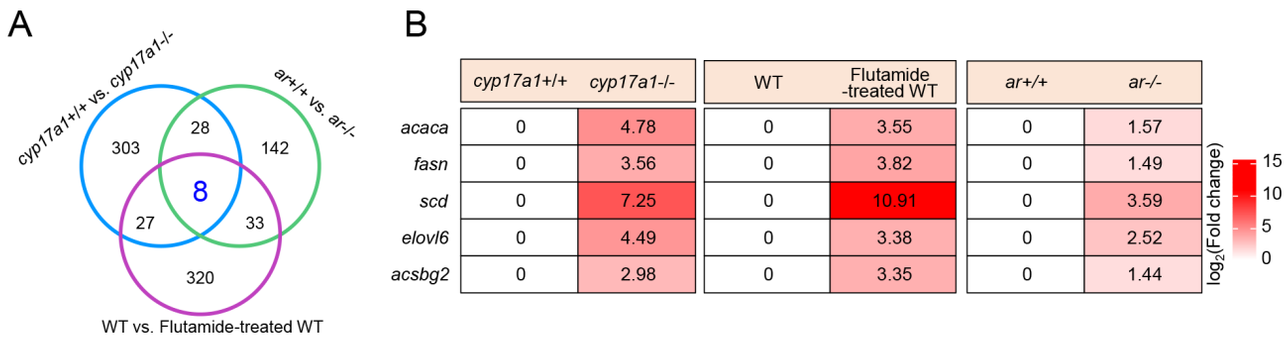

Figure 5 Analysis of hepatic DNL-related genes in *cyp17a1*-/-, *ar*-/-, and flutamide-treated WT fish

A: Venn analysis of hepatic RNA-seq data of *cyp17a1*-/-, *ar*-/-, and flutamide-treated WT fish. B: Heatmap of co-expressed hepatic DNL-related genes in *cyp17a1*-/-, *ar*-/-, and flutamide-treated WT fish.

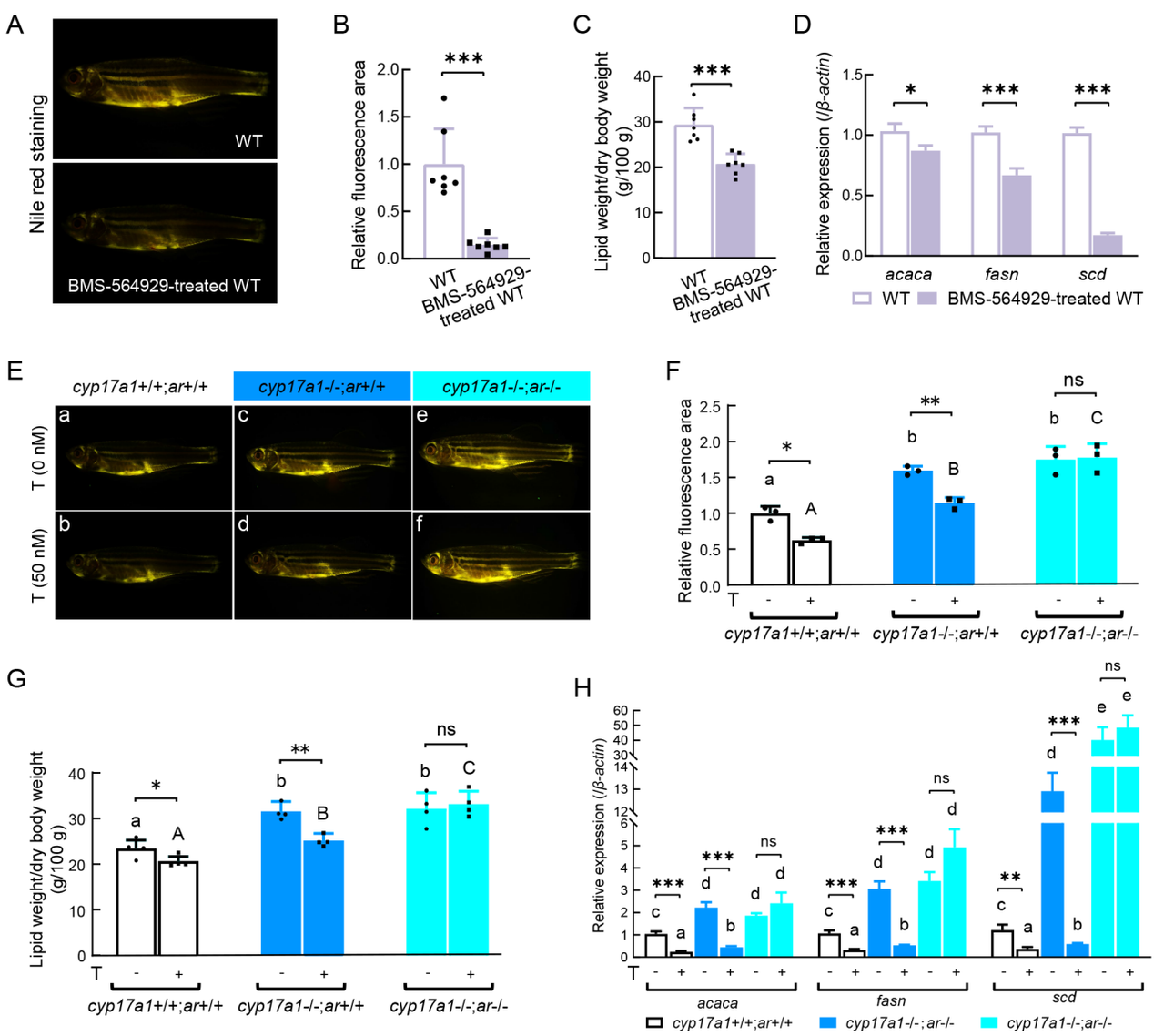

Figure 6 Testosterone inhibits VAT content, lipid content, and DNL gene expression via Ar

A: Nile red staining in male WT and BMS-564929-treated WT fish. B: Quantification of fluorescence area of Nile red staining in male WT and BMS-564929-treated WT fish (*n*=7/group). C: Whole-body lipid content in male WT and BMS-564929-treated WT fish (*n*=7/group). D: qPCR of hepatic DNL-related genes in male WT and BMS-564929-treated WT fish (*n*=4/group). E: Nile red staining of vehicle- or testosterone-treated male *cyp17a1*+/+;*ar*+/+, *cyp17a1*-/-;*ar*+/+, and *cyp17a1*-/-;*ar*-/- fish. F: Quantification of fluorescence area of Nile red staining in vehicle- or testosterone-treated male *cyp17a1*+/+;*ar*+/+, *cyp17a1*-/-;*ar*+/+, and *cyp17a1*-/-;*ar*-/- fish (*n*=3/group). G: Whole-body lipid content in vehicle- or testosterone-treated male *cyp17a1*+/+;*ar*+/+, *cyp17a1*-/-;*ar*+/+, and *cyp17a1*-/-;*ar*-/- fish (*n*=4/group). H: qPCR of hepatic DNL-related genes in vehicle- or testosterone-treated male *cyp17a1*+/+;*ar*+/+, *cyp17a1*-/-;*ar*+/+, and *cyp17a1*-/-;*ar*-/- fish (*n*=5/group). T, testosterone. Data represent mean±SD. ns: Not significant; *: $P<0.05$; **: $P<0.01$; ***: $P<0.001$.

Zhai et al., 2022). In *cyp17a1*-/- fish, male differentiation is compromised due to reduced testosterone and estradiol following the loss of 17α-hydroxylase and 17, 20-lyase activities of Cyp17a1 during gonadal steroidogenesis, as well as increased progestin signaling (Tokarz et al., 2013; Zhai et al., 2022). Conversely, *ar* depletion in zebrafish causes female-biased differentiation, male infertility via defective spermatogenesis, and premature ovarian failure during growth. This approach allows for the study of androgen signaling without interference from elevated progestin signaling and estrogen deficiency observed in *cyp17a1*-/- fish (Yu et al., 2018).

In the current study, the *cyp17a1*-/- and *ar*-/- fish models exhibited significant increases in VAT, lipid content, and visceral mass TG content (Figures 1, 3B–E). The DNL pathway is involved in the synthesis of fatty acids from excess nutrients such as carbohydrates and amino acids. Here, DNL-related genes showed significant differential expression in male *cyp17a1*-/- and *ar*-/- fish compared to their respective controls (Figures 1F, H, 3F, G). Furthermore, the activities of key enzymes involved in hepatic DNL were increased in *cyp17a1*-/- and *ar*-/- male fish (Figures 1I, 3I). Notably, the expression level of *scd*, which promotes the conversion of stearic acid (C18:0) to oleic acid (C18:1) in the DNL process (Hulver et al., 2005; Ntambi, 1999), was markedly elevated in *cyp17a1*-/- and *ar*-/- fish (Figures 1F, G, 3G, H). The stearic to oleic desaturation index (C18:1/C18:0) was also elevated in *cyp17a1*-/- fish, indicating increased Scd activity *in vivo*, aligning with the significant up-regulation in *scd* gene expression (Figure 1J). The observed up-regulation in fatty acid synthesis is supported by the coordinated changes in DNL gene expression, enzyme activity, and metabolite content in the livers of the *cyp17a1*-/- and *ar*-/- fish, suggesting that androgen signaling inhibits fatty acid synthesis in zebrafish.

Treatment with the Ar antagonist flutamide (Peets et al., 1974) successfully replicated the phenotypes seen in *cyp17a1*-/- and *ar*-/- males when applied to WT male zebrafish (Table 2). Venn analysis of the hepatic RNA-seq datasets from *cyp17a1*-/- fish (compared to *cyp17a1*+/+ males), *ar*-/- fish (compared to *ar*+/+ males), and flutamide-treated WT fish (compared to WT males) revealed that five of the eight significant co-regulated genes overlapping across these groups were associated with DNL (Figure 5A–B). The testosterone and Ar agonist BMS-564929 (Ostrowski et al., 2007) reduced VAT and lipid content and down-regulated *acaca*, *fasn*, and *scd* expression (Figure 6). Specifically, testosterone treatment in *cyp17a1*-/- fish effectively rescued the phenotypes mentioned above; however, the rescuing effect was abolished when *ar* was additionally depleted in *cyp17a1*-/-;*ar*-/- fish (Figure 6E–H). These findings demonstrate that androgen alleviates lipid deposition via activation of Ar through endogenous androgen signaling, underscoring that disruption in androgen signaling results in lipid deposition and up-regulation of DNL genes.

Venn analysis identified 23 genes with significant changes in both the RNA-seq and ATAC-seq datasets, with *fasn* and *scd* among the 11 genes found to be co-up-regulated (Figure 2H, I). These findings imply that androgen signaling may inhibit the transcriptional expression of the DNL pathway genes *fasn* and *scd* in zebrafish. However, determining whether this suppression is directly mediated remains challenging, as potential intermediate factors have not been excluded. To advance our understanding of the connection between androgen signaling and the DNL pathway, future studies should apply ChIP-seq with Ar antibodies to identify possible intermediate factors linking these signaling pathways.

Interestingly, observations revealed a higher body weight, food consumption, and basal oxygen intake in *cyp17a1*-/- fish compared to *cyp17a1*+/+ fish (Figure 1A; Supplementary Figure S2A, C). This pattern of weight gain following *cyp17a1* depletion is consistent with our recent study on common carp (*Cyprinus carpio*) (Zhai et al., 2021) and observations in *cyp17a1*-knockout;XX mice (Aherrahrou et al., 2020), suggesting a link between inactivated androgen signaling and increased body weight in both mammals and teleosts, although the underlying mechanism is still unknown. Additionally, elevated food intake and increased basal oxygen consumption were observed in *ar*-/- male zebrafish (Supplementary Figure S2B, D), indicating that androgen signaling may indeed play a role in suppressing zebrafish appetite. In contrast, our previous studies on *pomca*-deficient male zebrafish documented increased testosterone, body weight, and food intake, with significant adiposity in *pomca*-/- fish only emerging after depletion of *cyp17a1* (*pomca*-/-; *cyp17a1*-/- zebrafish) (Shi et al., 2020), indicating that increased levels of testosterone prevent lipid accumulation in *pomca*-/- zebrafish, despite the increase in body weight.

Locomotor activity remained unchanged at 6 h postprandial, with the distances traveled by *cyp17a1*-/- fish at slow, moderate, and high speeds comparable to those of *cyp17a1*+/+ fish (Supplementary Figure S3A–C). To further isolate factors potentially influencing lipid metabolism, lipid content was compared between *cyp17a1*-/- and *ar*-/- male fish with body weight-matched *cyp17a1*+/+ and *ar*+/+ male fish. Elevated lipid levels were still observed in the *cyp17a1*-/- and *ar*-/- male fish compared to their body weight-matched controls (Supplementary Tables S1, S5). These results refute the notion that lipid accumulation in *cyp17a1*-/- fish is due to a reduction in metabolic rate, reduced exercise capacity, or increased food intake.

Taken together, our study highlights the inhibitory effects of androgen signaling on hepatic DNL in zebrafish models with impaired androgen signaling. The fatty acids synthesized through DNL can serve as a storage as body fuel (Jump, 2011). High levels of hepatic DNL are implicated in high body lipid accumulation in cavefish (Xiong et al., 2022), suggesting

Table 2 Comparisons between *cyp17a1*-/-, *ar*-/-, and flutamide-treated WT fish with their control siblings

Group	*cyp17a1*+/+	*cyp17a1*-/-	*ar*+/+	*ar*-/-	WT	Flutamide-treated WT
Body weight (g)	0.2759±0.0552	0.3308±0.0757***	0.1984±0.0362	0.2472±0.0258 ***	0.4649±0.0403	0.4347±0.0429ns
Lipid content (%)	24.59±4.22	31.55±4.21***	20.02±1.63	24.75±3.36***	30.55±3.38	38.55±4.42***
Food intake (%)	23.76±2.82	36.40±3.13***	23.13±5.11	38.31±5.50 **	nd	nd
TG (visceral mass, mmol/g protein)	2.9812±0.5125	4.4293±0.3359***	2.2072±0.3948	2.9700±0.2417***	nd	nd
TG (Muscle, mmol/g protein)	0.1713±0.0353	0.1719±0.0284ns	0.2352±0.0331	0.2585±0.0349ns	nd	nd

TG, triglyceride. Data represent mean±SD. ns: Not significant; **: $P<0.01$; ***: $P<0.001$; nd: not determined.

that enhanced hepatic DNL may be an important contributor to the lipid mass increase observed in *cyp17a1*-/- and *ar*-/- zebrafish relative to their control siblings. Further exploration of the underlying molecular mechanisms mediating hepatic DNL and the androgen signaling pathway, along with the precise contribution of hepatic DNL to fish body lipid mass, will enhance our understanding of the regulatory roles of androgen signaling in fish metabolism beyond its reproductive functions.

DATA AVAILABILITY

Raw data, including the RNA-seq and ATAC-seq reads, were deposited in the National Center for Biotechnology Information database (PRJNA994675), Genome Sequence Archive (GSA: CRA014428), and Science Data Bank database (DOI: 10.57760/sciencedb.j00139.00103). The mass spectrometry data are available via MetaboLights under the identifier: MTBLS8518 (https://www.ebi.ac.uk/metabolights/editor/study/MTBLS8518).

SUPPLEMENTARY DATA

Supplementary data to this article can be found online.

COMPETING INTERESTS

The authors declare that they have no competing interests.

AUTHORS' CONTRIBUTIONS

J.J. conducted most of the experiments for this work. G.C. and T.S. provided help in fish breeding, rearing, and genotyping. Q.L., X.J., and J.H. provided help in data analyses. W.X. provided the *ar* knockout line. Z.Y. and G.Z. provided insights into this work and initiated and supervised the research team. J.J. and G.Z. wrote the manuscript. Z.Y. revised the paper. All authors read and approved the final version of the manuscript.

ACKNOWLEDGMENTS

We thank Mr. Wen-You Chen from the Institute of Hydrobiology, Chinese Academy of Sciences, for taking care of the zebrafish stocks.

REFERENCES

Aherrahrou R, Kulle AE, Alenina N, et al. 2020. CYP17A1 deficient XY mice display susceptibility to atherosclerosis, altered lipidomic profile and atypical sex development. *Scientific Reports*, **10**(1): 8792.

Beisaw A, Kuenne C, Guenther S, et al. 2020. AP-1 contributes to chromatin accessibility to promote sarcomere disassembly and cardiomyocyte protrusion during zebrafish heart regeneration. *Circulation Research*, **126**(12): 1760−1778.

Bekaert M, Van Nieuwenhove Y, Calders P, et al. 2015. Determinants of testosterone levels in human male obesity. *Endocrine*, **50**(1): 202−211.

Blouin K, Veilleux A, Luu-The V, et al. 2009. Androgen metabolism in adipose tissue: recent advances. *Molecular and Cellular Endocrinology*, **301**(1-2): 97−103.

Broughton DE, Moley KH. 2017. Obesity and female infertility: potential mediators of obesity's impact. *Fertility and Sterility*, **107**(4): 840−847.

Buenrostro JD, Giresi PG, Zaba LC, et al. 2013. Transposition of native chromatin for fast and sensitive epigenomic profiling of open chromatin, DNA-binding proteins and nucleosome position. *Nature Methods*, **10**(12): 1213−1218.

Buenrostro JD, Wu BJ, Chang HY, et al. 2015. ATAC-seq: a method for assaying chromatin accessibility genome-wide. *Current Protocols in Molecular Biology*, **109**: 21.29.1−21.29.9.

Chang C, Yeh S, Lee SO, et al. 2013. Androgen receptor (AR) pathophysiological roles in androgen-related diseases in skin, bone/muscle, metabolic syndrome and neuron/immune systems: lessons learned from mice lacking AR in specific cells. *Nuclear Receptor Signaling*, **11**: e001.

Chen QL, Luo Z, Pan YX, et al. 2013. Differential induction of enzymes and genes involved in lipid metabolism in liver and visceral adipose tissue of juvenile yellow catfish *Pelteobagrus fulvidraco* exposed to copper. *Aquatic Toxicology*, **136–137**: 72–78.

De Gendt K, Verhoeven G. 2012. Tissue- and cell-specific functions of the androgen receptor revealed through conditional knockout models in mice. *Molecular and Cellular Endocrinology*, **352**(1-2): 13−25.

Divers SL, McQuillan HJ, Matsubara H, et al. 2010. Effects of reproductive stage and 11-ketotestosterone on LPL mRNA levels in the ovary of the shortfinned eel. *Journal of Lipid Research*, **51**(11): 3250−3258.

Fan WQ, Yanase T, Nomura M, et al. 2005. Androgen receptor null male mice develop late-onset obesity caused by decreased energy expenditure and lipolytic activity but show normal insulin sensitivity with high adiponectin secretion. *Diabetes*, **54**(4): 1000−1008.

Folch J, Lees M, Stanley GHS. 1957. A simple method for the isolation and purification of total lipides from animal tissues. *Journal of Biological Chemistry*, **226**(1): 497−509.

Fui MNT, Dupuis P, Grossmann M. 2014. Lowered testosterone in male obesity: mechanisms, morbidity and management. *Asian Journal of Andrology*, **16**(2): 223−231.

Hoyos CM, Yee BJ, Phillips CL, et al. 2012. Body compositional and cardiometabolic effects of testosterone therapy in obese men with severe obstructive sleep apnoea: a randomised placebo-controlled trial. *European Journal of Endocrinology*, **167**(4): 531−541.

Hulver MW, Berggren JR, Carper MJ, et al. 2005. Elevated stearoyl-CoA desaturase-1 expression in skeletal muscle contributes to abnormal fatty acid partitioning in obese humans. *Cell Metabolism*, **2**(4): 251−261.

Jump DB. 2011. Fatty acid regulation of hepatic lipid metabolism. *Current Opinion in Clinical Nutrition and Metabolic Care*, **14**(2): 115−120.

Karbowska J, Kochan Z. 2013. Effects of DHEA on metabolic and endocrine functions of adipose tissue. *Hormone Molecular Biology and Clinical Investigation*, **14**(2): 65−74.

Kelly DM, Jones TH. 2013. Testosterone: a metabolic hormone in health and disease. *Journal of Endocrinology*, **217**(3): R25−R45.

Kim D, Paggi JM, Park C, et al. 2019. Graph-based genome alignment and genotyping with HISAT2 and HISAT-genotype. *Nature Biotechnology*, **37**(8): 907−915.

Li LY, Lv HB, Jiang ZY, et al. 2020. Peroxisomal proliferator-activated receptor α-b deficiency induces the reprogramming of nutrient metabolism in zebrafish. *The Journal of Physiology*, **598**(20): 4537−4553.

Livak KJ, Schmittgen TD. 2001. Analysis of relative gene expression data using real-time quantitative PCR and the 2-ddCT method. *Methods*, **25**(4): 402−408.

Lopes C, Madureira TV, Ferreira N, et al. 2016. Peroxisome proliferator-activated receptor gamma (PPARγ) in brown trout: Interference of estrogenic and androgenic inputs in primary hepatocytes. *Environmental Toxicology and Pharmacology*, **46**: 328−336.

Lopes C, Rocha E, Pereira IL, et al. 2021. Deciphering influences of testosterone and dihydrotestosterone on lipid metabolism genes using brown trout primary hepatocytes. *Aquatic Toxicology*, **235**: 105819.

Love MI, Huber W, Anders S. 2014. Moderated estimation of fold change and dispersion for RNA-seq data with DESeq2. *Genome Biology*, **15**(12): 550.

Luo LH, Gribskov M, Wang SF. 2022. Bibliometric review of ATAC-Seq and its application in gene expression. *Briefings in Bioinformatics*, **23**(3): bbac061.

Nikolaenko L, Jia Y, Wang C, et al. 2014. Testosterone replacement ameliorates nonalcoholic fatty liver disease in castrated male rats. *Endocrinology*, **155**(2): 417−428.

Ntambi JM. 1999. Regulation of stearoyl-CoA desaturase by polyunsaturated fatty acids and cholesterol. *Journal of Lipid Research*,

40(9): 1549−1558.

O'Reilly MW, House PJ, Tomlinson JW. 2014. Understanding androgen action in adipose tissue. *The Journal of Steroid Biochemistry and Molecular Biology*, **143**: 277−284.

Ostrowski J, Kuhns JE, Lupisella JA, et al. 2007. Pharmacological and x-ray structural characterization of a novel selective androgen receptor modulator: Potent hyperanabolic stimulation of skeletal muscle with hypostimulation of prostate in rats. *Endocrinology*, **148**(1): 4−12.

Park PJ. 2009. ChIP-seq: advantages and challenges of a maturing technology. *Nature Reviews Genetics*, **10**(10): 669−680.

Peets EA, Henson MF, Neri R. 1974. On the mechanism of the anti-androgenic action of flutamide (α-α-α-trifluoro-2-methyl-4'-nitro-m-propionotoluidide) in the rat. *Endocrinology*, **94**(2): 532−540.

Powell-Wiley TM, Poirier P, Burke LE, et al. 2021. obesity and cardiovascular disease: A scientific statement from the American Heart Association. *Circulation*, **143**(21): e984−e1010.

Rubio-Almanza M, Cámara-Gómez R, Merino-Torres JF. 2019. Obesity and type 2 diabetes: Also linked in therapeutic options. *Endocrinología, Diabetes y Nutrición*, **66**(3): 140−149.

Safaei M, Sundararajan EA, Driss M, et al. 2021. A systematic literature review on obesity: Understanding the causes & consequences of obesity and reviewing various machine learning approaches used to predict obesity. *Computers in Biology and Medicine*, **136**: 104754.

Sangiao-Alvarellos S, Polakof S, Arjona FJ, et al. 2006. Influence of testosterone administration on osmoregulation and energy metabolism of gilthead sea bream *Sparus auratus*. *General and Comparative Endocrinology*, **149**(1): 30–41.

Sato T, Matsumoto T, Yamada T, et al. 2003. Late onset of obesity in male *androgen receptor*-deficient (AR KO) mice. *Biochemical and Biophysical Research Communications*, **300**(1): 167−171.

Shi C, Lu Y, Zhai G, et al. 2020. Hyperandrogenism in POMCa-deficient zebrafish enhances somatic growth without increasing adiposity. *Journal of Molecular Cell Biology*, **12**(4): 291−304.

Sun SX, Cao XJ, Castro LFC, et al. 2021. A network-based approach to identify protein kinases critical for regulating *srebf1* in lipid deposition causing obesity. *Functional & Integrative Genomics*, **21**(5-6): 557−570.

Sunny F, Jacob A, Oommen OV. 2002. Sex steroids regulate intermediary metabolism in *Oreochromis mossambicus*. *Endocrine Research*, **28**(3): 175–188.

Tan BB, Zhang Y, Zhang TT, et al. 2020. Identifying potential serum biomarkers of breast cancer through targeted free fatty acid profiles screening based on a GC-MS platform. *Biomedical Chromatography*, **34**(10): e4922.

Tchernof A, Brochu D, Maltais-Payette I, et al. 2018. Androgens and the regulation of adiposity and body fat distribution in Humans. *Comprehensive Physiology*, **8**(4): 1253−1290.

Team RC. 2021. R: A language and environment for statistical computing. Vienna: R Foundation for Statistical Computing.

Tokarz J, Möller G, De Angelis MH, et al. 2013. Zebrafish and steroids: what do we know and what do we need to know?. *The Journal of Steroid Biochemistry and Molecular Biology*, **137**: 165−173.

Tonstad S, Després JP. 2011. Treatment of lipid disorders in obesity. *Expert Review of Cardiovascular Therapy*, **9**(8): 1069−1080.

Ubhayasekera SJKA, Staaf J, Forslund A, et al. 2013. Free fatty acid determination in plasma by GC-MS after conversion to Weinreb amides. *Analytical and Bioanalytical Chemistry*, **405**(6): 1929−1935.

Wang W, Zhu H, Tian ZH, et al. 2020. Effects of 11-Ketotestosterone on development of the previtellogenic ovary in the Sterlet. *Acipenser ruthenus. Frontiers in Endocrinology*, **11**: 115.

Westerfield M. 2020. The zebrafish book, a guide for the laboratory use of zebrafish (*Danio rerio*). Eugene: University of Oregon.

WHO. 2000. Obesity: preventing and managing the global epidemic: Report of a WHO consultation. Geneva: World Health Organization.

Xi LW, Zhai G, Liu YL, et al. 2023. Attenuated glucose uptake promotes catabolic metabolism through activated AMPK signaling and impaired insulin signaling in zebrafish. *Frontiers in Nutrition*, **10**: 1187283.

Xiong SL, Wang W, Kenzior A, et al. 2022. Enhanced lipogenesis through Pparγ helps cavefish adapt to food scarcity. *Current Biology*, **32**(10): 2272−2280.e6.

Yanase T, Fan WQ, Kyoya K, et al. 2008. Androgens and metabolic syndrome: lessons from *androgen receptor* knock out (ARKO) mice. *The Journal of Steroid Biochemistry and Molecular Biology*, **109**(3-5): 254−257.

Yang BY, Zhai G, Gong YL, et al. 2018. Different physiological roles of insulin receptors in mediating nutrient metabolism in zebrafish. *American Journal of Physiology-Endocrinology and Metabolism*, **315**(1): E38−E51.

Yu GC, Wang LG, Han YY, et al. 2012. clusterProfiler: an R package for comparing biological themes among gene clusters. *Omics:A Journal of Integrative Biology*, **16**(5): 284−287.

Yu GC, Wang LG, He QY. 2015. ChIPseeker: an R/Bioconductor package for ChIP peak annotation, comparison and visualization. *Bioinformatics*, **31**(14): 2382−2383.

Yu GQ, Zhang DW, Liu W, et al. 2018. Zebrafish androgen receptor is required for spermatogenesis and maintenance of ovarian function. *Oncotarget*, **9**(36): 24320−24334.

Zhai G, Shu TT, Chen KX, et al. 2021. Successful production of an all-female common carp (*Cyprinus carpio* L.) population using *cyp17a1*-deficient neomale carp. *Engineering*, **8**: 181−189.

Zhai G, Shu TT, Xia YG, et al. 2017. Androgen signaling regulates the transcription of *anti-Müllerian hormone* via synergy with SRY-related protein SOX9A. *Science Bulletin*, **62**(3): 197−203.

Zhai G, Shu TT, Xia YG, et al. 2018. Characterization of sexual trait development in *cyp17a1*-deficient zebrafish. *Endocrinology*, **159**(10): 3549−3562.

Zhai G, Shu TT, Yu GQ, et al. 2022. Augmentation of progestin signaling rescues testis organization and spermatogenesis in zebrafish with the depletion of androgen signaling. *eLife*, **11**: e66118.

Zhang DK, Wei YH, Huang QN, et al. 2022. Important hormones regulating lipid metabolism. *Molecules*, **27**(20): 7052.